

Integral field spectroscopy of selected areas of the Bright Bar and Orion-S cloud in the Orion Nebula^{*}

A. Mesa-Delgado^{†1,2,3}, M. Núñez-Díaz^{2,3}, C. Esteban^{2,3}, L. López-Martín^{2,3} and J. García-Rojas^{2,3}

¹*Institute for Astronomy, 2680 Woodlawn Drive, Honolulu, HI 96822, USA*

²*Instituto de Astrofísica de Canarias, E-38200 La Laguna, Tenerife, Spain*

³*Departamento de Astrofísica, Universidad de La Laguna, E-38205 La Laguna, Tenerife, Spain*

Accepted 2011 June 16. Received 2011 June 13; in original form 2011 May 12

ABSTRACT

We present integral field spectroscopy of two selected zones in the Orion Nebula obtained with the Potsdam Multi-Aperture Spectrophotometer (PMAS), covering the optical spectral range from 3500 to 7200 Å and with a spatial resolution of 1''. The observed zones are located on the prominent Bright Bar and on the brightest area at the northeast of the Orion South cloud, both containing remarkable ionization fronts. We obtain maps of emission line fluxes and ratios, electron density and temperatures, and chemical abundances. We study the ionization structure and morphology of both fields, which ionization fronts show different inclination angles with respect to the plane of the sky. We find that the maps of electron density, O⁺/H⁺ and O/H ratios show a rather similar structure. We interpret this as produced by the strong dependence on density of the [O II] lines used to derive the O⁺ abundance, and that our nominal values of electron density –derived from the [S II] line ratio– may be slightly higher than the appropriate value for the O⁺ zone. We measure the faint recombination lines of O II in the field at the northeast of the Orion South cloud allowing us to explore the so-called abundance discrepancy problem. We find a rather constant abundance discrepancy across the field and a mean value similar to that determined in other areas of the Orion Nebula, indicating that the particular physical conditions of this ionization front do not contribute to this discrepancy.

Key words: ISM: abundances, H II regions – ISM: individual objects: Orion Nebula

1 INTRODUCTION

The analysis of H II regions is currently our best tool to study the physical conditions and chemical abundances of the interstellar medium. Because of its proximity and high surface brightness, the Orion Nebula (M42) is one of the best studied H II regions of our galaxy. Although the Orion Nebula has a large extension for more than one half degree, most of the radiation comes from the inner part, the so-called Huygens region. This is an active star-formation region ionized by a group of four massive stars known as the Trapezium cluster, where θ^1 Ori C (O7 V; Simón-Díaz et al. 2006) is the main ionizing source and, therefore, responsible of the bulk

of nebular emission from the main ionization front (MIF). Physical, chemical, kinematical and structural properties for this H II region have been studied in depth using different observational techniques (*e.g.* Hester et al. 1991; Pogge et al. 1992; Walter et al. 1992; Esteban et al. 1998; Bally et al. 2000; O'Dell 2001; O'Dell et al. 2003; Doi et al. 2004; Esteban et al. 2004; García-Díaz & Henney 2007; García-Díaz et al. 2008; O'Dell & Henney 2008; O'Dell et al. 2009) as well as photoionization models (*e.g.* Zuckerman 1973; Balick et al. 1974; Rubin et al. 1991; Baldwin et al. 1991; Wen & O'Dell 1995; O'Dell 2001). The presence of many different morphological features such as protoplanetary discs, Herbig-Haro objects or bright bars makes the Orion Nebula the best laboratory for analysing photoionization phenomena.

Their study of ionization fronts is one of these phenomena of special interest because they are transitions between the fully ionized gas and its neutral surroundings, where we expect density and temperature gradients. Probably, there

^{*} Based on observations collected at the Centro Astronómico Hispano Alemán (CAHA) at Calar Alto, operated jointly by the Max-Planck Institut für Astronomie and the Instituto de Astrofísica de Andalucía (CSIC).

[†] E-mail: amd@ifa.hawaii.edu/adalfis@gmail.com

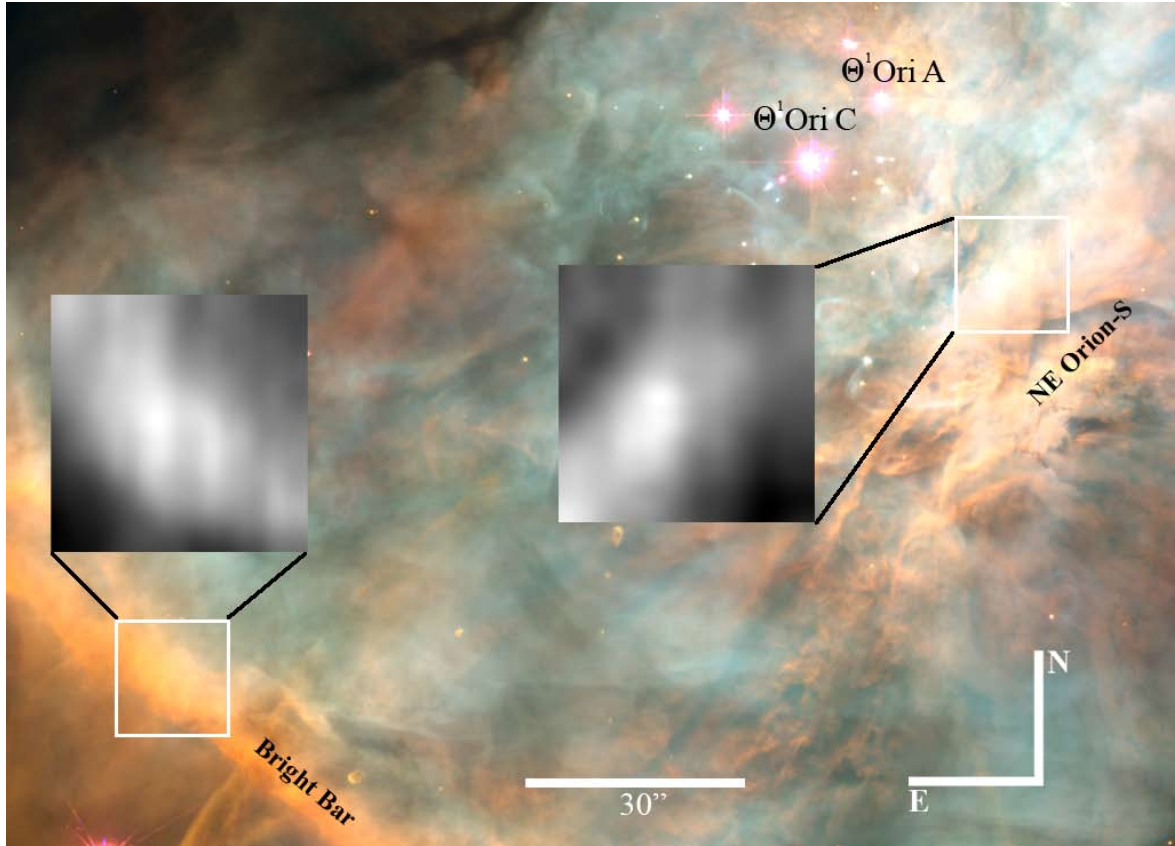


Figure 1. *HST* image of the central part of the Orion Nebula, which combines WFPC2 images taken in different narrow-band filters (O’Dell & Wong 1996). The white squares correspond to the fields of view of PMAS IFU used, covering the Bright Bar and the northeast edge of the Orion-S cloud (NE-Orion-S). The black and white images show enlargements of the $H\alpha$ emission in our PMAS fields, rebinned to 160×160 pixels and smoothed using a Gaussian filter.

is an ionization front in almost every direction towards the Orion Nebula, though only certain geometries allow us to explore the ionization structure of these features. The clearest example in the Orion Nebula is the well-known Bright Bar (hereinafter, BB). It is one of the most conspicuous features of the Orion Nebula, which is seen as an elongated structure in both ionized gas and molecular emission. It is located at about $111''$ to the southeast of $\theta^1\text{Ori C}$. The BB appears specially bright in emission lines of low ionization species such as $[\text{N II}]$ or $[\text{S II}]$ (e.g. Hester 1991; Pogge et al. 1992; Walter et al. 1993; García-Díaz & Henney 2007). On the basis of this fact, Balick et al. (1974) proposed that the BB is an escarpment in the MIF. Multi-wavelength studies from infrared to radio spectral domains as well as theoretical modeling (e.g. Tielens et al. 1993; Tauber et al. 1994; van der Werf et al. 1996; Marconi et al. 1998; Young Owl et al. 2000; Kassis et al. 2006; van der Wiel et al. 2009; Pellegrini et al. 2009, and references therein) support this proposal, where the MIF changes from a face-on to an edge-on geometry. Pellegrini et al. (2009) modeled the emission spectra along the transition from H^+ to H^0 and H_2 regions. They adopt a thin slab geometry for the BB, which extends 0.115 pc and is inclined 7° with respect to the line of sight, finding a good agreement between the computed optical spectrum and that observed by Baldwin et al. (1991).

Besides the BB, there are other remarkable areas in the Orion Nebula. Recently, García-Díaz & Henney (2007)

have identified several examples of compact bars toward the core of the Huygens region, in addition to the brighter bars previously reported in the literature (O’Dell & Yusef-Zadeh 2000). This is the case of the brightest zone of the Huygens region (see Fig. 1), located at the northeast at the north-east edge of the Orion South (Orion-S) cloud (hereinafter, NE-Orion-S). This region is located about $30''$ to the southwest of $\theta^1\text{Ori C}$. In several observational studies (e.g. Pogge et al. 1992; Walter et al. 1993; García-Díaz & Henney 2007) the NE-Orion-S appears as an extended structure, which is very bright in $[\text{N II}]$ and $[\text{S II}]$ emission lines as in the case of the BB. Recently, O’Dell et al. (2009) have studied in-depth the three dimensional structure of the whole Orion-S concluding that it is a cloud ionized from one side facing to $\theta^1\text{Ori C}$ and suspended within the main body of the Orion Nebula in front of the MIF. Therefore, this cloud as well as its NE-Orion-S edge are ionization fronts with a given unknown inclination, though it should not be as tilted as the BB (O’Dell et al. 2009).

As we will see in the next paragraphs, there have been a number of works devoted to study the spatial distributions of physical conditions and chemical abundances in the Orion Nebula, but this is the first one specifically dedicated to these ionization fronts –BB and NE-Orion-S– making use of integral field spectroscopy in the optical spectral range at spatial scales of about $1''$. Walter et al. (1992) determined radial gradients of the physical conditions from the analysis of

Table 1. Journal of observations.

Field	α^a	δ^a	Exposure time (s)	
			-72° Blue	-68° Red
Bright Bar	05 ^h 35 ^m 22 ^s .3	-05 [°] 24' 33''0	4×600,1×10	1×300,1×10
NE-Orion-S	05 ^h 35 ^m 14 ^s .5	-05 [°] 23' 36''0	1×400,1×10	1×300,1×10

^a Coordinates of the field centre (J2000.0).

22 different areas of the nebula obtained from long-slit spectrophotometry. Pogge et al. (1992) and Walter et al. (1993) studied the ionization structure of the entire Huygens region by means of Fabry-Perot and CCD imaging, respectively. Pogge et al. (1992) obtained the first electron density map, finding the maximum values precisely at the NE-Orion-S position. More recently, O'Dell et al. (2003) carried out a high-spatial resolution map of the electron temperature (derived from the [O III] line ratio) centered at the southwest of the Trapezium cluster from flux-calibrated narrow-band images taken with the Hubble Space Telescope (*HST*). Rubin et al. (2003) also analysed long-slit data taken with *STIS* at the *HST*, obtaining the spatial distributions of electron temperatures (derived from the [O III] and [N II] line ratios) along 4 slit positions. Using long-slit spectroscopy at spatial scales of $1''.2$ and covering the Huygens region with 5 slit positions, Mesa-Delgado et al. (2008) also obtained the spatial distributions of emission lines fluxes, physical conditions and chemical abundances, specially of those derived from faint recombination lines of heavy-element ions. There are just a few works using integral field spectroscopy in the Orion Nebula. Sánchez et al. (2007) obtained a mosaic of the Orion Nebula from integral field spectroscopy with a spatial resolution of $2''.7$ but with very short exposure times. The electron temperature map obtained by these authors from the [N II] line ratio shows spatial variations and the electron density map is very rich in substructures. There are only three additional studies available in the literature that used this observational technique in small fields of the Orion Nebula, though they are focused in the analysis of certain morphological structures. These are the cases of Vasconcelos et al. (2005) and Tsamis et al. (2011), who study the protoplanetary disc LV2, and Mesa-Delgado et al. (2009), focused in the study of the prominent Herbig-Haro object HH 202.

In §2 we describe the observations made with PMAS and the reduction procedure. In §3 we describe the emission line measurements and the reddening correction of the spectra. In §4 we explain the calculations of physical conditions and chemical abundances. In §5 we present the spatial distributions of the flux of several emissions lines and emission line ratios, physical conditions and chemical abundances. In §6 we discuss the structure of the two ionization fronts studied as well as the so-called abundance discrepancy problem. Finally, in §7 we summarize our main conclusions.

2 OBSERVATIONS AND DATA REDUCTION

In Fig. 1 we show the two fields on the Orion Nebula observed in service time on 2008 December 19-20 at Calar Alto Observatory (Almería, Spain). Integral field spectroscopy was performed in these fields using the Potsdam Multi-Aperture Spectrophotometer (PMAS, Roth et al. 2005) at

the 3.5-m Telescope and its standard lens array integral field unit (IFU) of $16'' \times 16''$ field of view (FoV) with a spaxel size of $1'' \times 1''$. The optical range from 3500 to 7200 Å was covered using the V600 grating and two rotator angles (-72° for the blue spectra and -68° for the red one). This grating allowed us to achieve an effective spectral resolution of about 3.6 Å. The total integration times for the blue and red spectra as well as the central coordinates of each field are presented in Table 1. Additional short exposures of 10 seconds were also taken in order to avoid saturation of the brightest emission lines. Calibration images were also obtained during the night: HgNe arc lamps for the wavelength calibration and continuum lamps needed to extract the 256 individual spectra on the CCD. The PMAS data were reduced (bias subtraction, spectra extractions and flat-fielding correction) as well as wavelength and flux calibrated using the IRAF¹ reduction package SPECRED (see Mesa-Delgado et al. 2009, for more details on the reduction process). The data were calibrated using the spectrophotometric standard stars Feige 100, Feige 34, Feige 110 and G 191-B2B (Oke 1990) and the error of the absolute flux calibration was about 5%. The night reports indicated the presence of thin clouds during the observations of the BB, and this could be the most likely reason of a disagreement of about 15% in the absolute flux measurements between the short and long time exposures of the BB in the red range. We corrected for this effect and we do not expect that the final results are substantially affected because we only use emission line ratios in our analyses. This correction was also considered in the calculation of the flux measurement errors (see §3.1) for the spectra of this range and field. In the blue range of the BB field we found a difference between the short and long exposure spectra lower than 3% (even lower than the nominal error in the flux calibration). For the NE-Orion-S, the differences between the short and large exposures were also lower than 3% along the whole wavelength coverage in both blue and red spectral ranges. The seeing had an average value of about $1''.5$ during the observations.

The integral field data cubes are subject to the effects of the differential atmospheric refraction (DAR) along the direction of the parallactic angle. This effect was corrected using our own IDL routines (similar to the previous ones written by P.T. Wallace for STARLINK and Walsh & Roy 1990) implementing the method outlined by Hohenkerk & Sinclair (1985) (see also §3.281 of Seidelmann 1992). The procedure calculates the fractional spaxel shifts for each monochromatic image with respect to a given wavelength. The maximum DAR shift was obtained for the BB field reaching values of $\Delta\alpha = 0''.62$ and $\Delta\delta = 1''.16$ between [O II] 3727

¹ IRAF is distributed by NOAO, which is operated by AURA, under cooperative agreement with NSF.

Å and H β . The reference wavelengths were H β and H α for the blue and red data cube, respectively. These emission lines were also used to align the blue and red data cubes calculating the right spaxel offsets that produce the maximum correlation between both H β and H α emission maps. For the two fields, these offsets reached values lower than 0".3 in α and δ . Finally, the data cubes are corrected using the BILINEAR function of IDL, the calculated fractional shifts and the alignment offsets. As result of all this process, the maximum coincident FoV resulting in the whole wavelength range is reduced to 14" \times 14". We tested the DAR correction observing the alignment of localized features at different H I lines finding good agreement in all cases.

3 LINE MEASUREMENTS AND REDDENING CORRECTION

3.1 Line intensity measurements

We measured the intensity of all the emission lines needed to perform our analysis: hydrogen Balmer lines (from H α to H12), which are used to compute the reddening correction and verify the DAR correction; collisionally excited lines (CELs) of different species (see §4.2), which are needed to compute physical conditions and chemical abundances; and, finally, the faint C II and O II lines, which are used to derive the ionic abundances from recombination lines (RLs). It should be mentioned that both RLs were only detected in the NE-Orion-S field. These faint lines were not detected in the BB due to its lower surface brightness and lower ionization degree. In Fig. 2, we present the spectra of a representative spaxel, $(-1:-2,5:6)^2$, of the NE-Orion-S, where we can see the blend of O II 4649, 4651 Å lines used to derive the O²⁺/H⁺ ratio.

The measurement of the emission line fluxes were performed applying a single or a multiple, in the cases where it was necessary, Gaussian profile fit procedure between two given limits and over the local continuum making use of the SPLOT routine of IRAF. All measurements of the bright lines were made with our own scripts to automatize the process. However, the flux of the faint C II 4267 Å and O II 4650 Å lines of the NE-Orion-S field were measured by hand for each individual spaxel. We have determined the errors in the flux measurements following the criteria defined by Mesa-Delgado et al. (2008). The final error for each emission line was the result of the quadratic sum of the flux measurement error and the flux calibration error. As in our previous publications, we defined three criteria to avoid spurious weak line measurements in the automatic procedure and to discriminate between real features and noise: 1) line intensity peak over 2.5 times the sigma of the local continuum; 2) FWHM(H I)/1.5 < FWHM(λ) < 1.5 \times FWHM(H I); and 3) F(λ) > 0.0001 \times F(H β).

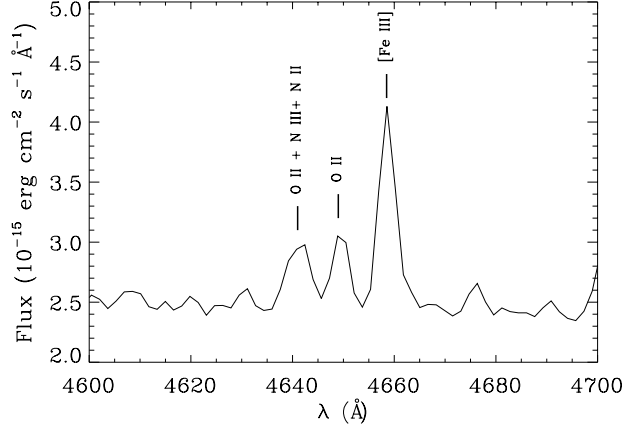


Figure 2. Section of a PMAS spectrum around O II lines of multiplet 1 corresponding to the spaxel position $(-1:-2,5:6)$ of the NE-Orion-S field. The O II feature at about 4650 Å corresponds to the blend of O II 4649, 4651 Å lines. The O II + N III + N II feature corresponds to the blend of O II 4639, 4642 Å, N III 4641, 4642 Å, and N II 4643 Å lines.

3.2 Reddening correction

The reddening coefficient, $c(\text{H}\beta)$, was obtained by fitting the observed H γ /H β and H δ /H β ratios to the theoretical ones predicted by Storey & Hummer (1995) for $n_e = 1000 \text{ cm}^{-3}$ and $T_e = 10000 \text{ K}$. In a previous step, we considered more H I line ratios in the calculations, but they only added more dispersion to the final $c(\text{H}\beta)$ value because the rest of available lines were either rather faint (H11 and H12), or blended with other bright lines (the case of H7, H8 and H9). We used the updated reddening function, $f(\lambda)$, normalized to H β for the Orion Nebula ($R_V = 5.5$; Blagrove et al. 2007). The use of this extinction law instead of the classical one of Costero & Peimbert (1970) produces $c(\text{H}\beta)$ values about 0.1 dex higher and dereddened fluxes with respect to H β about 3% lower for lines in the range 5000 to 7500 Å, 4% higher for wavelengths below than 5000 Å and 2% for wavelengths above 7500 Å. The final adopted $c(\text{H}\beta)$ value for each spaxel is an average of the individual values derived from each Balmer line ratio weighted by their corresponding uncertainties. The typical error of $c(\text{H}\beta)$ is about 0.20 dex for each spaxel. All emission line fluxes of a given spectrum were normalized to H β and H α for the blue and red range, respectively. To produce a final homogeneous set of line flux ratios, all of them were re-scaled to H β after the reddening correction. The re-scaling factor used in the red spectra was the theoretical H α /H β ratio for the physical conditions of $T_e = 10000 \text{ K}$ and $n_e = 1000 \text{ cm}^{-3}$.

The resulting extinction maps are shown in Figs 3a and 3b for the BB and NE-Orion-S, respectively. The extinction coefficients vary approximately from 0.4 to 1.0 dex for the two fields. In the case of the BB, the highest values, 0.9 and 1.0 dex, are located at the southeast corner of the field, while the lowest values are found at the position of the ionization front in the middle of the field. The NE-Orion-S

² Hereinafter, the localization of an individual spaxel or multiple spaxels will be given as (X1:X2,Y1:Y2) according to the coordinate system used in the maps presented in next sections.

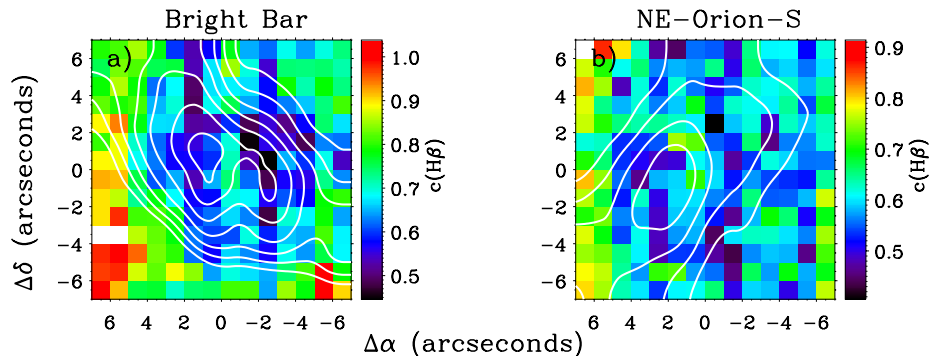


Figure 3. Spatial distribution maps of the extinction coefficient, $c(H\beta)$, with $H\alpha$ contours overplotted for the two PMAS fields: a) Bright Bar and b) NE-Orion-S.

presents values between 0.5 to 0.7 dex in most of the field and somewhat larger values –between 0.7 and 0.9 dex– at the east edge of the observed area. We have estimated the mean $c(H\beta)$ value of each field as well as the standard deviation, which amounts to 0.7 ± 0.2 and 0.6 ± 0.1 dex for the BB and NE-Orion-S, respectively. These mean values are in agreement with other determinations available in the literature. O’Dell & Yusef-Zadeh (2000) obtained $c(H\beta)$ maps and derived consistent $c(H\beta)$ values both from the $H\alpha/H\beta$ line ratio by using calibrated *HST* images and from radio to optical surface brightness ratio. Using their extinction maps, we have found $c(H\beta)$ values ranging from 0.4 to 0.6 for the BB and 0.4 to 0.7 for the NE-Orion-S at the precise positions of our fields. These extinction values of O’Dell & Yusef-Zadeh (2000) were determined using the classical extinction law of Costero & Peimbert (1970) and, as we commented before, should be increased by about 0.1 dex to be compared with our determinations.

4 DETERMINATIONS OF PHYSICAL CONDITIONS AND CHEMICAL ABUNDANCES

4.1 Physical conditions

We have used the TEMDEN task of the NEBULAR package of IRAF (Shaw & Dufour 1995) with updated atomic data (see García-Rojas et al. 2009), to determine the physical conditions, electron densities, n_e , and temperatures, T_e , for each spaxel of our PMAS fields from the usual CEL ratios –[S II] 6717/6731 Å for n_e , and [O III] (4959+5007)/4363 Å and [N II] (6548+6584)/5755 Å for T_e . For these calculations, we have followed the same procedure described in Mesa-Delgado et al. (2008) assuming an initial $T_e = 10000$ K to obtain a first approximation of n_e , then we calculate $T_e([O III])$ and $T_e([N II])$, and iterate until convergence. We have not considered the contribution by recombination in the observed flux of the auroral line [N II] 5755 Å to derive $T_e([N II])$, because it is very small for the conditions of the Orion Nebula (e.g. Esteban et al. 2004). The typical uncertainties in the density maps of the BB range from 1000 to 1200 cm^{-3} . For the NE-Orion-S field, the typical error in the density distribution amounts to 4000 cm^{-3} . This higher error is due to the much higher densities at this particular area of the nebula (e.g. Pogge et al. 1992; Wen & O’Dell 1995;

Mesa-Delgado et al. 2008), that makes the [S II] indicator to be about the high density limit. The typical error for electron temperatures range from 500 to 1000 K for $T_e([N II])$ and from 100 to 200 K in the case of $T_e([O III])$.

4.2 Chemical abundances

We have derived abundances for several ions from CELs: N^+ , O^+ , O^{2+} , S^+ , S^{2+} , Ne^{2+} and Ar^{2+} making use of the IRAF task IONIC of the package NEBULAR. We have assumed a two-zone scheme and adopting $T_e([N II])$ for low ionization potential ions (N^+ , O^+ and S^+) and $T_e([O III])$ for high ionization potential ones (O^{2+} , S^{2+} , Ne^{2+} and Ar^{2+}). We have computed the ionic abundance errors as the quadratic sum of independent contributions from n_e , T_e , and line flux uncertainties. For ionic and total abundances of oxygen, the average uncertainties are 0.12-0.20 dex for O^+/H^+ , 0.03 dex for O^{2+}/H^+ and 0.10-0.15 dex for O/H .

In addition, we have also detected and measured pure RLs of O II and C II in the majority of spaxels covering the NE-Orion-S field (see Fig. 2). RLs have the advantage that their relative fluxes with respect to H I lines depend weakly on T_e and n_e , avoiding the problem of the possible presence of temperature and/or density fluctuations. These fluctuations can be actually affecting the abundance determinations from CELs, whose emissivities strongly depend on the physical conditions of the ionized gas (Peimbert 1967).

The spectral resolution of our spectra does not allow to separate the blend of the two brightest individual lines of multiplet 1 of O II at 4649 and 4651 Å. In this situation, the combination of equations (1) and (4) by Peimbert & Peimbert (2005) should be used to determine the O^{2+} abundance from these RLs. These expressions permit to correct the line fluxes from NLTE effects in the relative intensity of the individual lines of the multiplet, though they are rather small in the Orion Nebula due to its relatively high density. Therefore, we have calculated the O^{2+}/H^+ ratio from RLs as:

$$\frac{O^{2+}}{H^+} = \frac{\lambda_{M1}}{4861} \times \frac{\alpha_{eff}(H\beta)}{\alpha_{eff}(M1)} \times \frac{I(M1 \text{ O II})}{I(H\beta)}, \quad (1)$$

where $\alpha_{eff}(H\beta)$ and $\alpha_{eff}(M1)$ are the effective recombination coefficients for $H\beta$ and for the O II multiplet 1, respectively, and $\lambda_{M1} = 4651.5$ Å the representative mean wavelength of the whole multiplet. We have also calculated the C^{2+}/H^+ ratio from the flux of C II 4267 Å RL and using

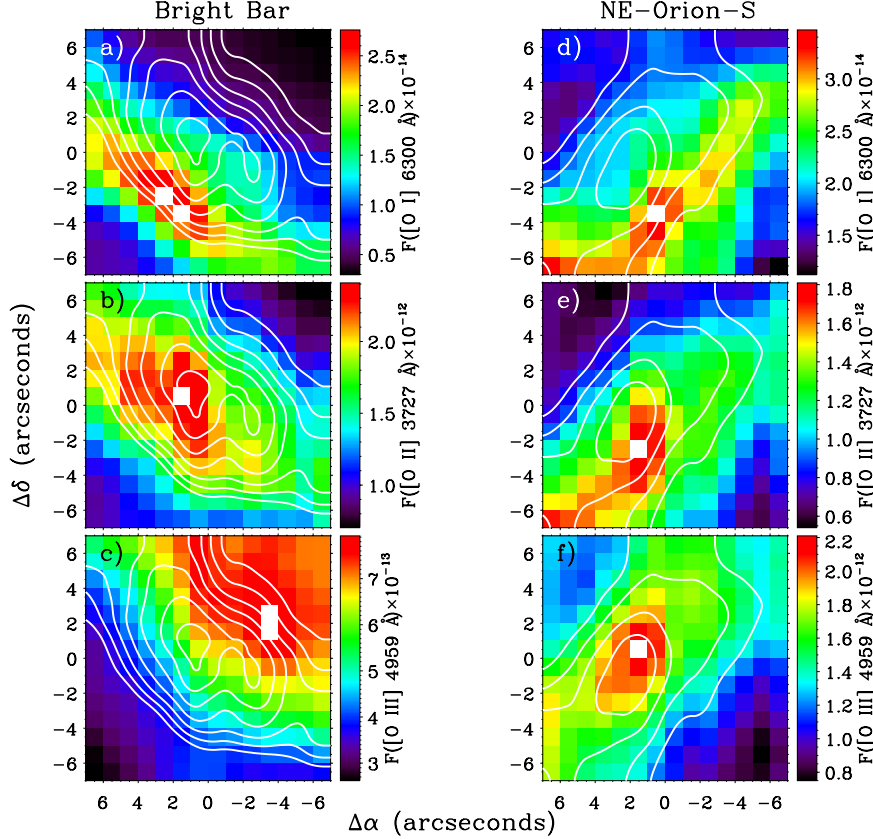


Figure 4. Spatial distributions of emission line fluxes in units of $\text{erg cm}^{-2} \text{s}^{-1}$ of the main ionization stages of oxygen at the conditions of the Orion Nebula: [O I] 6300 Å (top), [O II] 3727 Å (middle) and [O III] 4959 Å (bottom). The maps correspond to the Bright Bar (left) and NE-Orion-S (right) fields. $\text{H}\alpha$ contours are overplotted in all maps.

an analogous equation to (1) particularized for the case of this ion. According to the two-zone scheme, we have adopted $T_e([\text{O III}])$ to calculate the abundances of both ions, O^{2+} and C^{2+} . We have used the effective recombination coefficients of Storey 1994 to derive the O^{2+} abundances (assuming LS coupling) and Davey et al. 2000 for C^{2+} abundances. The typical errors in the abundances from RLs amount to 0.08-0.10 dex for C^{2+}/H^+ and 0.10-0.12 dex for O^{2+}/H^+ .

5 RESULTS: SPATIAL DISTRIBUTION MAPS

In this section we analyse the spatial distributions of several emission line fluxes, emission line ratios, electron densities and temperatures as well as abundances for several representative ions for each PMAS field.

5.1 Emission line fluxes and excitation ratios

In Fig. 4, we present the spatial distribution maps of [O I] 6300 Å, [O II] 3727 Å and [O III] 4959 Å emission line fluxes for both the BB (Figs 4a–4c) and NE-Orion-S (Figs 4d–4f). These maps show the distribution of the different ionic species of oxygen that can be found in the Orion Nebula: O^0 , O^+ and O^{2+} . As it can be seen, the ionization stratification of the two ionization fronts is clearly resolved in the maps. However, these maps are really showing a combination of

the ionization stratification and the density distribution of the gas because the emissivity of a line is proportional –at first order– to n_e^2 . It is very illustrative to compare these maps with those of the [O I]/ $\text{H}\alpha$, [N II]/ $\text{H}\alpha$ and [O III]/ $\text{H}\beta$ line ratios shown in Fig. 5. Line ratios are directly related to the local ionization degree of the gas and do not depend in a direct manner on density. In Fig. 5 we represent [N II]/ $\text{H}\alpha$ instead of [O II]/ $\text{H}\beta$ because the [N II]/ $\text{H}\alpha$ ratio is the most commonly used indicator for the analysis of ionization fronts and shows a very similar spatial distribution to [O II]/ $\text{H}\beta$. As it is explained in O’Dell et al. (2009), the [N II]/ $\text{H}\alpha$ ratio is a good indicator to detect when the MIF is tilted and, therefore, this is the reason that the BB is so well defined in Fig. 5.

As it has been said before, Figs 4–5 show the ionization stratification at and around the ionization fronts. In both figures, it is evident that the areas with the higher [O I] 6300 Å line emission and [O I]/ $\text{H}\alpha$ ratio are narrower than those of the other lines represented in the figures, and their maxima tend to be also located farther away with respect to $\theta^1 \text{Ori C}$ (see Fig. 1). We can notice some differences between the spatial distributions of line fluxes and ratios for the BB and NE-Orion-S. Firstly, the widths of the zones occupied by the tracers of the ionization fronts, [O I] and [N II], are narrower for the BB than for the NE-Orion-S. This indicates that the inclination angles of the planes of the fronts with respect to the line of sight of both features are different. In

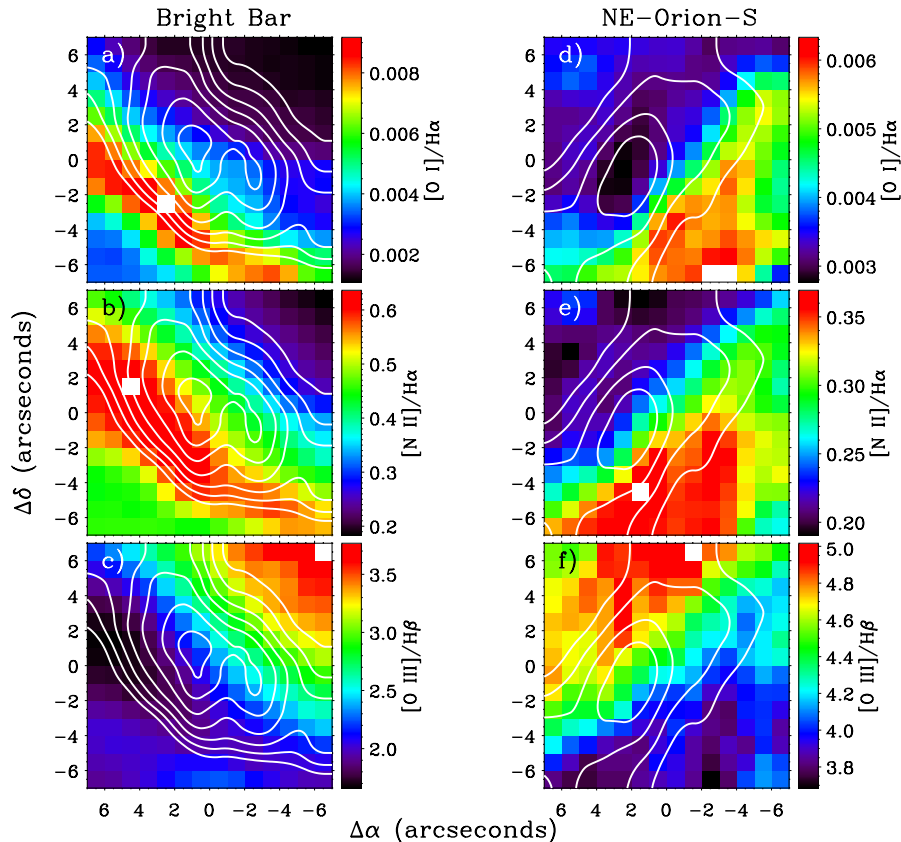


Figure 5. Spatial distribution maps of selected emission line ratios for the Bright Bar (left) and NE-Orion-S (right). The sum of [N II] 6548, 6584 Å and [O III] 4959, 5007 Å nebular lines have been used to derive the [N II]/H α (middle) and [O III]/H β (bottom) ratios, respectively. H α contours are overplotted in all maps.

fact, as we commented in §1, this was already suggested by O’Dell et al. (2009). The BB is located at a border of the Huygens region where the MIF is an edge-on escarpment, where its plane is tilted about 7° with respect to our line of sight (Pellegrini et al. 2009). The situation is not so clear in the case of the NE-Orion-S. It is a portion the Orion-S cloud, which is suspended in front of the MIF with an unknown inclination and can be interpreted as a bump in the otherwise concave surface of the MIF at the Huygens region (O’Dell et al. 2009). Secondly, another difference between the BB and NE-Orion-S can be seen comparing the maps shown in Figs 4 and 5. In the case of the BB, Fig. 4b) shows that the maxima of [O II] 3727 Å and H α emission coincide. However, in the case of the NE-Orion-S, Fig. 4f) indicates that the maximum of H α emission coincides with [O III] 4959 Å. This difference is due to the NE-Orion-S area is nearer to θ^1 Ori C than the BB and that while few photons capable of producing O $^{2+}$ are reaching the BB, NE-Orion-S is illuminated by a significant fraction of such high-energy photons. This is clearly confirmed in Fig. 5c), where the maximum of the [O III]/H β line ratio is well outside the BB and towards the ionizing source of the nebula. Interestingly, Fig. 5f) indicates that in the case of the NE-Orion-S, the zone of the highest [O III]/H β line ratio is just at the north edge of the field. This area coincides with a filament, which seems to be out of Orion-S cloud itself. Its higher excitation

suggests that this filament should be nearer to θ^1 Ori C and perhaps belongs to the MIF.

5.2 Physical conditions

In Fig. 6 we present the physical conditions for the two observed fields: n_e ([S II]), T_e ([N II]), T_e ([O III]) and the temperature ratio T_e ([N II])/ T_e ([O III]).

Both fields show n_e spatial variations of the order of a factor 2. The densities in the BB range from 3000 to 5500 cm $^{-3}$, but larger values are found in the NE-Orion-S, from 8000 to 16000 cm $^{-3}$. In the BB field, maximum densities are found within the H α contours, while in the NE-Orion-S these are displaced with respect to the maximum of H I emission. The average densities of the ionization fronts are 4370 ± 580 cm $^{-3}$ for the BB and 10900 ± 1900 cm $^{-3}$ for the NE-Orion-S. In the case of the NE-Orion-S field, the highest density values are about the high density limit of the [S II] line ratio indicator and, therefore, they may not correspond to the true densities. Fortunately, we have detected at least 5 [Fe III] lines of the 3F multiplet ([Fe III] 4607, 4658, 4702, 4734 and 4755 Å) and one line of the 2F multiplet ([Fe III] 4881 Å) at those spaxels of the NE-Orion-S field showing the n_e ([S II]) maxima. These lines permit to get an additional determination of the density, n_e ([Fe III]), which range of validity has an upper limit above that of the [S II] indicator. To carry out these calculations we have used a 34-level atom using

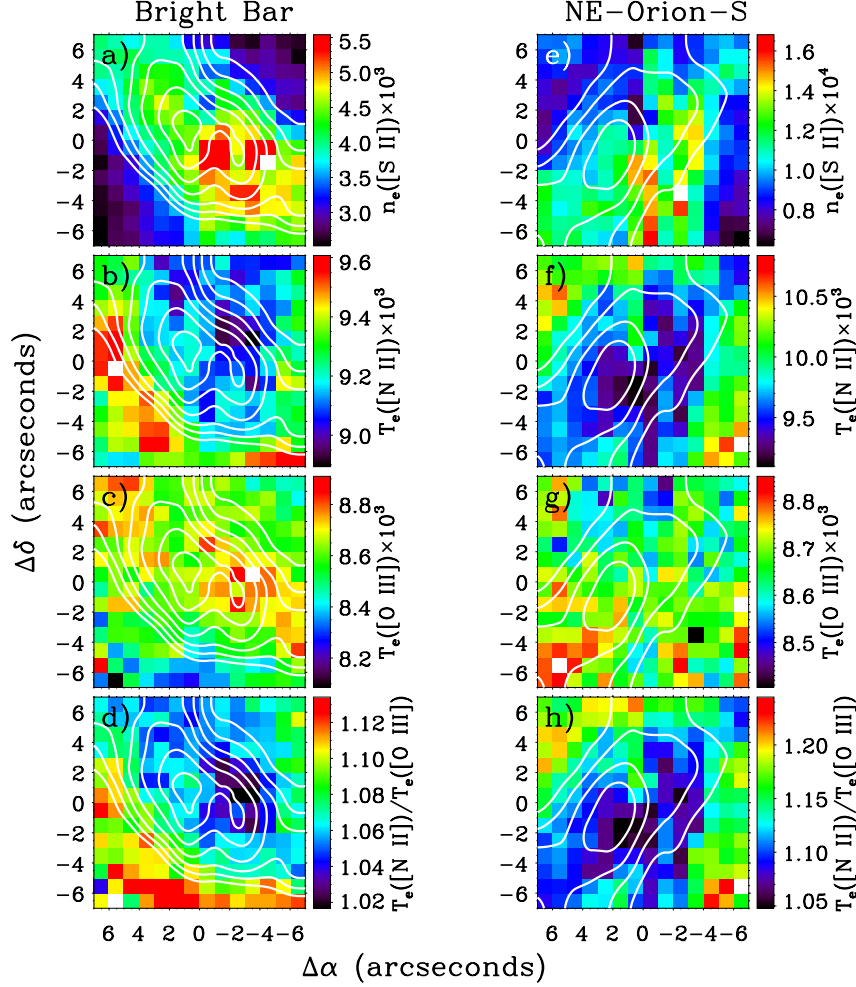


Figure 6. Spatial distributions of physical conditions for the Bright Bar (left column) and NE-Orion-S (right column). For all fields, we present $n_e([S II])$ (top row) in units of cm^{-3} , $T_e([N II])$ (second row from top) and $T_e([O III])$ (third row from top) in units of K, and the ratio of both temperatures (bottom row). $H\alpha$ contours are overplotted in all maps.

the collision strengths from Zhang (1996) and the transition probabilities of Quinet (1996) and Johansson et al. (2000). The calculations of $n_e([Fe III])$ give densities varying from 10000 to 18000 cm^{-3} , even though they have large uncertainties (between 3000 and 6000 cm^{-3}) due to the faintness of the $[Fe III]$ lines. The differences among the $n_e([Fe III])$ and $n_e([S II])$ determined for a given spaxel amount from 1% to 30%, and it is clear that these differences are within the uncertainties of both indicators. Therefore, the high $n_e([S II])$ we obtain in Fig. 6e) should be considered at least close to the true electron density of the ionized gas at the NE-Orion-S (further discussion of these results can be found in §5.3).

The spatial distributions of $T_e([N II])$ show a similar qualitative behaviour in both ionization fronts (Figs. 6b and 6f). The pattern seems to be almost inverse to the density distributions reaching the minimum temperatures approximately at the maximum densities. In the case of the BB, the range of variation of $T_e([N II])$ along the field is rather narrow reaching the maximum temperatures –about 9500 K– just at the outer edge of the bar. In the case of the NE-Orion-S field, the range of values of $T_e([N II])$ is wider and the temperatures are always higher than in the BB. The

maximum values of temperature are also found at the outer edge of the ionization fronts.

The spatial distributions of $T_e([O III])$ (Figs 6c and 6g) are rather featureless with mean values of about 8620 and 8670 K and variations of the order 600 and 400 K in the BB and NE-Orion-S fields, respectively. In both fields, the maximum values of $T_e([O III])$ tend to be located within the $H I$ emission. In the NE-Orion-S, we can see a zone of higher values located at the southwest corner of the field, though these values have also higher uncertainties –about 200-250 K.

In Figs 6d) and 6h) we present the $T_e([N II])/T_e([O III])$ ratio for both fields. As we can see, $T_e([N II])$ is always slightly higher than $T_e([O III])$. This is the expected behaviour in an ionization bounded nebula as a consequence of the hardening of the incident radiation field due to photoelectric absorption in the low ionization zones where the $[N II]$ lines are emitted. This ratio tends to be higher in the outer zones of both fronts.

We have compared our determinations of the physical conditions with previous ones available in the literature for the same or nearby areas. These are the cases of: the long-

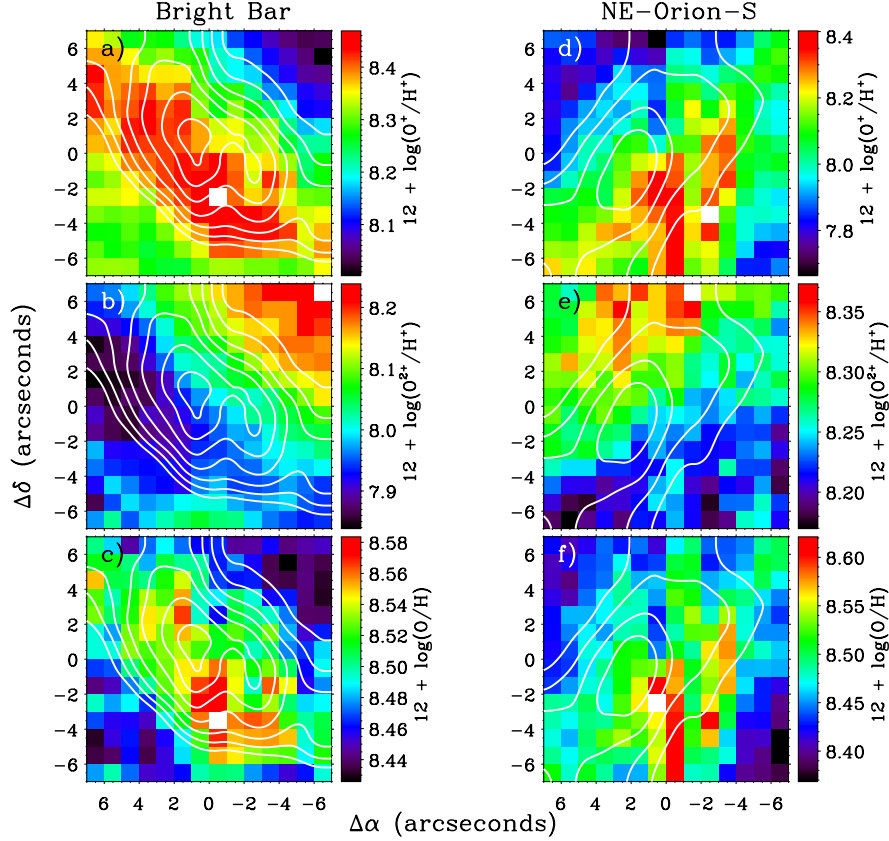


Figure 7. Spatial distributions of the O^+/H^+ , O^{2+}/H^+ and O/H ratios—in the usual logarithmic scale—for the Bright Bar (left column) and NE-Orion-S (right column). $\text{H}\alpha$ contours are overplotted in all maps.

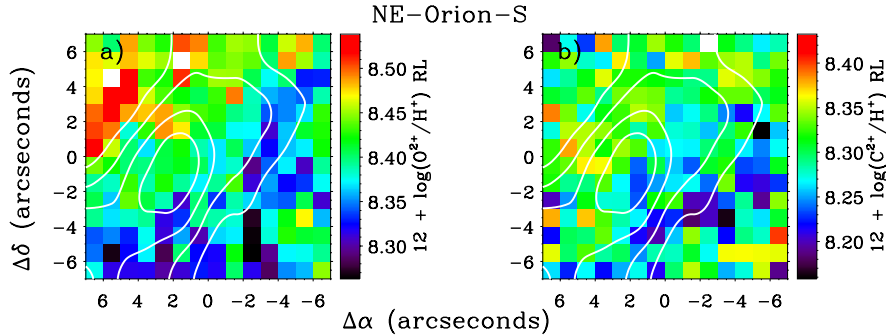


Figure 8. Spatial distributions of O^{2+} and C^{2+} abundances determined from recombination lines for the NE-Orion-S. $\text{H}\alpha$ contours are overplotted.

slit positions 1, 3, 4 and 5 analysed by Mesa-Delgado et al. (2008), which cover a small area of the Orion-S cloud and the BB; the long-slit positions 2 and 4 studied by Rubin et al. (2003), which cover some parts of both ionization fronts; several of the slit positions observed by Baldwin et al. (1991); the results presented by Pogge et al. (1992) for the whole Huygens region; and the results from the model of Wen & O'Dell (1995). In general, we have found a good agreement between the results obtained in these papers and our determinations, reproducing some of the patterns discussed in the previous paragraphs. However, we have found a slight disagreement with the n_e determinations of Pogge et al. (1992)

for the BB. These authors analysed a spatial profile of n_e crossing the BB in an area located about $40''$ to the southwest of our field and with a position angle of 150° . Their profile reaches densities of about 3200 cm^{-3} – 1000 cm^{-3} lower than our determination— but in agreement with the results by García-Díaz & Henney (2007) along a similar slit position. On the other hand, our density determination is in agreement with the model results of Wen & O'Dell (1995). In their figure 4a, they present a spatial profile of the density with a position angle of 322° , which precisely crosses our BB field, finding densities of about 5000 cm^{-3} , similar to our values. Therefore, the small differences found here be-

tween our physical conditions and those reported by other authors seem to be related to the presence of local variations of the physical conditions in the BB. Wen & O'Dell (1995), in their figure 5a, also presented a spatial profile of the density with a position angle of 226° covering the NE-Orion-S field, which passes close to the southeast corner of our field. They found densities no higher than 12000 cm^{-3} , slightly lower than our determinations but consistent within the uncertainties.

5.3 Chemical abundances

In Fig. 7 we present the spatial distributions of ionic and total oxygen abundances derived from CELs for the two fields. As expected, the O^+ and O^{2+} abundance distributions are rather similar to those of the $[\text{N II}]/\text{H}\alpha$ and $[\text{O III}]/\text{H}\beta$ line ratios shown in Fig. 5. However, unexpectedly, we find structures in the spatial distributions of the total O abundance of both fields as we can see in Figs 7c) and 7f). The mean values of the O/H ratio at the BB and NE-Orion-S amount to 8.49 ± 0.03 dex and 8.48 ± 0.05 dex, respectively, which are in complete agreement with the typical oxygen abundances -8.50 dex– obtained by previous works in different parts of the Orion Nebula (Esteban et al. 1998, 2004; Blagrove et al. 2006; Mesa-Delgado et al. 2009; Simón-Díaz & Stasińska 2011). In the BB field, the O abundance variations are within the typical error of about 0.10-0.15 dex, while in the NE-Orion-S the range is slightly wider, finding the lowest values at the southwest corner of the field, precisely where the O^{2+} abundances are lower and $T_e([\text{O III}])$ has a larger uncertainty, as we mentioned in §5.2. In Fig. 7, we can see that the areas with the highest total O abundance coincide in general with those showing higher O^+/H^+ ratio. Moreover, the structure of the spatial variations of the O/H ratio shown in Figs 7c) and 7f) is remarkably similar to that of the n_e maps of Figs 6a) and 6e). To understand this behaviour we have to consider that ionic abundance determinations derived from CELs depend very much on the physical conditions of the gas. O^+/H^+ and O^{2+}/H^+ ratios are both strongly dependent on T_e , but not on n_e at the same level. In particular, the O^+/H^+ ratio derived from the $[\text{O II}]$ 3727 Å doublet is much more dependent on n_e than the O^{2+} abundance calculated from the nebular $[\text{O III}]$ 4959, 5007 Å lines at least at the densities measured in our PMAS fields. Therefore, the striking similar structure of the O/H and n_e maps may be produced by the strong dependence of the O^+ abundance on n_e . The simpler explanation is that the $n_e([\text{S II}])$ we obtain for the ionization fronts is not indicating the true density of the O^+ zone and, therefore, not appropriate for determining the O^+ abundances. A possible way to check this solution could be to obtain high-spectral resolution spectra to measure and separate the $[\text{O II}]$ 3726, 3729, 7319 and 7330 Å lines and derive the precise physical conditions of the O^+ zone. Another explanation is that, even in the case that the physical conditions are the same for S^+ and O^+ , $n_e([\text{S II}])$ could not be the true one because the reported densities are about –specially in the case of NE-Orion-S– the critical densities of the $[\text{S II}]$ 6717, 6731 Å lines ~ 2000 - 3000 cm^{-3} and 10000 cm^{-3} , respectively. In fact, considering densities somewhat higher than the true values produce higher O^+/H^+ ratios. This is because we overestimate the collisional de-excitation affecting the $[\text{O II}]$ line

Table 2. Average distances^a from the peaks of the selected emission lines with respect to that of $[\text{O I}]$

	Bright Bar	NE-Orion-S
$[\text{S II}]$	$1''0 \pm 0''4$	$0''4 \pm 0''5$
$[\text{O II}]$	$2''3 \pm 0''9$	$1''4 \pm 1''1$
H I	$4''5 \pm 1''0$	$3''1 \pm 1''1$
He I	$5''5 \pm 0''9$	$3''3 \pm 0''8$
$[\text{O III}]$	$7''6 \pm 1''1$	$3''9 \pm 0''8$

^a Each value is given as $\langle x \rangle \pm \sigma$.

fluxes. Furthermore, $[\text{O II}]$ 3726, 3729 Å emission flux can be affected in the same way than $[\text{S II}]$ lines due to they have similar critical densities $\sim 3000 \text{ cm}^{-3}$ and 5000 cm^{-3} , respectively. Assuming that the main contribution comes from using a wrong density, we have estimated by which amount we have to correct n_e in order to obtain the mean nominal value of the O abundance of the Orion Nebula -8.50 dex– in the zones of our fields with higher O^+/H^+ ratio. This exercise gives that densities about 1000 and 4000 cm^{-3} lower than those determined for the BB and NE-Orion-S fields, respectively, are enough to wash out the problem. These values are rather modest and of the order or even smaller than the uncertainties estimated for $n_e([\text{S II}])$ and $n_e([\text{Fe III}])$ in each field (§4.1). Higher signal-to-noise ratio $[\text{Fe III}]$ spectra and/or good determinations of other indicators with higher critical densities such as $\text{C II}]$ 2326, 2328 Å, $[\text{Cl III}]$ 5517, 5537 Å or even $\text{C III}]$ 1907, 1909 Å, as well as the observation of $[\text{O II}]$ 7319, 7330 Å to derive O^+ abundances would be necessary to disentangle this situation.

Finally, in Fig. 8, we present the O^{2+} and C^{2+} abundances derived from RLs for the NE-Orion-S, the only field where these emission lines were satisfactorily detected and measured. From the comparison of Fig. 7e) and Fig. 8a), we can see that the spatial distributions of O^{2+}/H^+ determined from CELs and RLs show a rather similar behaviour, placing the maximum abundance values at the spaxels of the northeast corner, where the gas of higher excitation is located. Ionic abundance maps from RLs are noisier than those from CELs due to the faintness of the RLs. As it is common in ionized nebulae, we find that the O^{2+} abundances determined from RLs are higher than those from CELs, which is related to the abundance discrepancy problem as we will discuss in §6.2

6 DISCUSSION

6.1 Structure of the ionization fronts

In this section we study the ionization fronts of the two observed fields. With this aim, we analyse the spatial profiles of emission lines emitted from ions with different ionization potentials (O^0 , S^+ , O^+ , H^+ , He^+ and O^{2+}). We have extracted the spatial profiles from cuts roughly parallel to the radial direction to $\theta^1 \text{ Ori C}$, connecting the southeast with the northwest corner in the BB field and the southwest with the northeast corner in the NE-Orion-S field. The use of all possible profiles along these directions allowed us to statistically determine the relative distance between the maximum of the spatial distribution of the $[\text{O I}]$ emission and the other

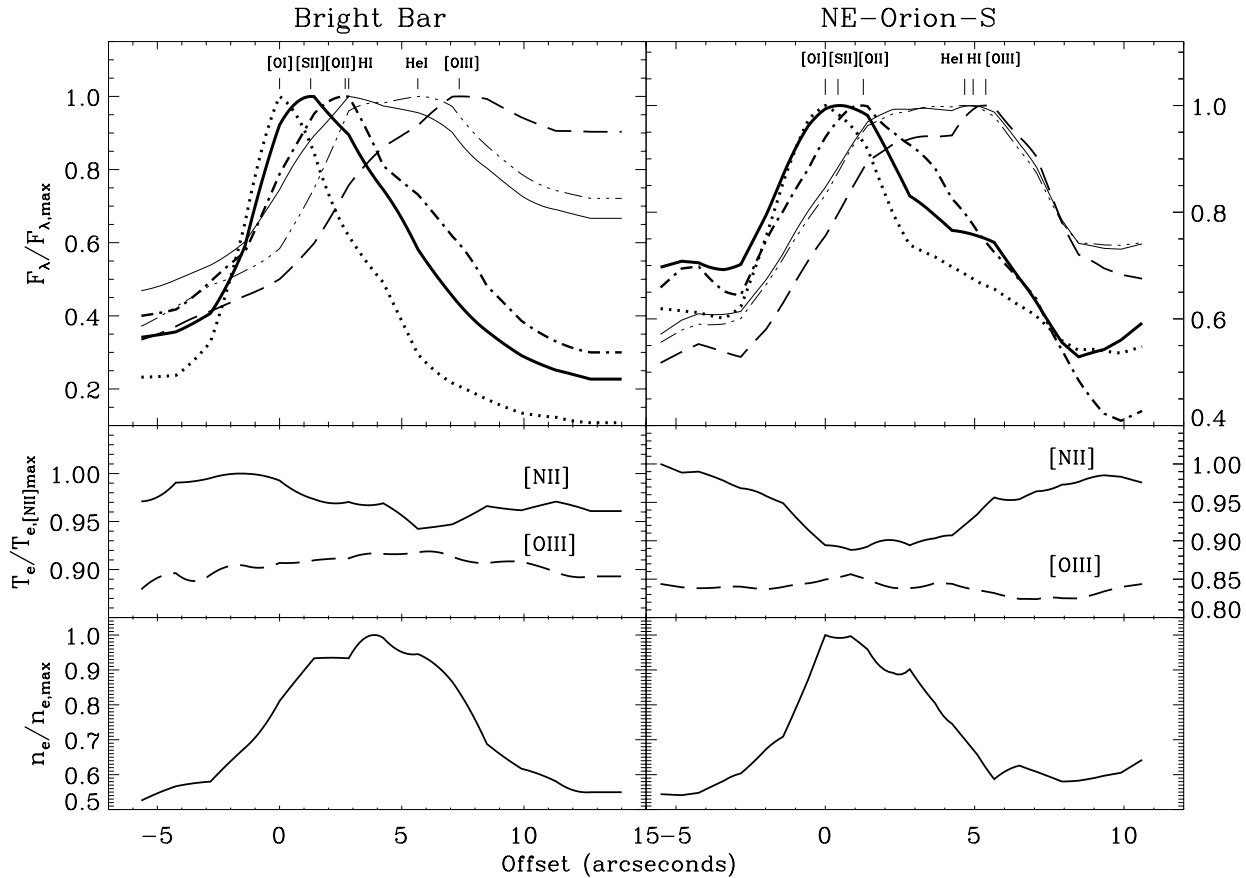


Figure 9. Spatial profiles of several emission lines traced along the main diagonal from the southeast to the northwest corner of the Bright Bar (top left) and along the third line below (to the southeast) of the main diagonal from the southwest to the northeast corner of the NE-Orion-S (top right). The zero point is located at the maximum of [O I] line emission and the offsets are given in arcseconds on the plane of the sky. Positive values in abscissae indicate decreasing distance with respect to θ^1 Ori C. The plotted lines are: [O I] (dotted line), [S I] (black solid line), [O II] (dashed-dotted line), H I (thinner solid line), He I (three dotted-dashed line) and [O III] (dashed line). The emission line fluxes are normalized to their maximum emission. In the middle and bottom panels, the spatial profiles of T_e ([N II]) (solid line) and T_e ([O III]) (dashed line), as well as n_e ([S II]) are presented. T_e ([N II]) and n_e ([S II]) are normalized to their respective maxima: 9480 K and 4760 cm^{-3} for the Bright Bar and 10390 K and 14200 cm^{-3} for the NE-Orion-S.

emission lines across the fields. To estimate these distances, we have used the rebinned maps without applying any Gaussian smoothing filter as we did for the $H\alpha$ images presented in Fig. 1. The rebinned maps do not change the relative positions of the maxima and allow us to explore the changes in the profiles interpolating at subarcsecond scales. Furthermore, these maps allow to use a total of 29 spatial profiles to calculate statistically significant averages. In Table 2 we present the average values of these distances and their standard deviations. In Fig. 9 we present spatial profiles of the emission lines only for one representative cut: along the main diagonal in the case of the BB; and along the third diagonal line towards the southeast of the main diagonal in the case of the NE-Orion-S. In Fig. 9 we also show the temperature and density distributions along the same cuts. For all profiles, we have located the zero point at the position of the maximum of [O I] emission, which is the farthest one from θ^1 Ori C, as we saw in Fig. 4 and see now in Fig. 9.

Theory about the ionization structure of nebulae can be found in Osterbrock & Ferland (2006). In our discussion below, we state that the stratification should be driven by the ionization energy of the atom. This is approximately true,

but it should also be mentioned that the local ionizing radiation field in a nebula, which control the distribution of the ionic states of heavy elements, is determined by the opacity of the two most abundant elements, hydrogen and helium. In terms of the emission lines fluxes presented in Fig. 9, this implies that both [O I] and [S II] arise near the zone where hydrogen becomes optically thick and the presence of these ions is combined with thermalized electrons coming from hydrogen photoionizations. [O II] as well as [N II] emissions arise from the zone where hydrogen is ionized and helium is still neutral. Finally, [O III] emission comes from the nearest zone to θ^1 Ori C, where hydrogen remains ionized and helium is once ionized. In the spatial profiles presented in Fig. 9, the small differences with respect to that expected stratification are probably a combined effect of the geometry of each ionization front and the density dependence of the observed flux.

The ionization structure of the BB has been well studied in the literature (*e.g.* Hester 1991; Tielens et al. 1993; Walmsley et al. 2000; Pellegrini et al. 2009; van der Wiel et al. 2009). This bar is basically edge-on and its plane has an inclination of 7° with respect to the line of sight (Pel-

legrini et al. 2009), allowing to resolve its ionization structure as we see in Fig. 9. The MIF is a thin layer located between the maximum emission peaks of [O I] and [S II]. Pellegrini et al. (2009) indicate that the maxima of H₂ and ¹²CO line emissions are detected at about 12'' and 20'' behind the MIF position, respectively. As we see in Table 2, we found that the peak of the [S II] emission is located about 1'' ahead [O I], which corresponds to a physical separation of 2.1×10^{-3} pc assuming a distance to the Orion Nebula of 436 ± 20 pc (O'Dell & Henney 2008). The maximum of [O II] emission, which also coincides with the maxima of [N II] (14.5 eV) and [Fe III] (16.2 eV), is found about $2''.3 - 4.9 \times 10^{-3}$ pc— with a standard deviation of 0''.9, implying that this zone is spatially less defined than that of [S II] emission. The spatial profiles of the H I and He I emission lines are more extended. The mean distance of the peak of H I emission is $4''.5$ (9.5×10^{-3} pc) with a standard deviation of 1''. In the case of He I emission, its maximum is located between the H I and [O III] zones—as it is expected considering the ionization potential of this ion (24.6 eV)— at $5''.5$ (11.6×10^{-3} pc) with respect to the peak of [O I] emission. The He I emission distribution represented in Fig. 9 corresponds to the line at 6678 Å, which permits to avoid problems related to self-absorption due to it comes from a singlet state. Finally, the [O III] zone reaches its maximum value at $7''.6$ (16.1×10^{-3} pc).

In contrast to the BB, the ionization structure of NE-Orion-S has not been described in the literature. Taking into account the distances estimated in Table 2, the distribution of the spatial profiles shown in Fig. 9 and comparing with the results for the BB, it is clear that we can not resolve the ionization structure of the NE-Orion-S as well as of the BB because this front is much tilted with respect to the line of sight. In their figure 5b, Wen & O'Dell (1995) present the geometry of their Orion Nebula model along a cut with a position angle of 226° , which passes close to the southeast corner of our NE-Orion-S field. At a distance of 30'' from the center of our field, the model by Wen & O'Dell (1995) indicates that the MIF has an inclination of about 60° with respect to the line of sight and after that the MIF remains rather parallel to the plane of the sky. The properties of the nebular structure to whom NE-Orion-S belongs, the Orion-S cloud, have been recently reviewed by O'Dell et al. (2009) showing that it should be located in the foreground with an unknown inclination as well as an uncertain placement in the three-dimensional space, but at a similar distance with respect to θ^1 Ori C as that of the MIF in the background (0.182 pc). The inclination angle of the NE-Orion-S have to be such to produce the observed distances between line emission maxima given in Table 2, where, on the one hand, the emission of [S II] and [O II] and, on the other hand, the emissions of H I, He I and [O III] are not well separated at our spatial resolution. We can compare the data of Table 2 for the BB and NE-Orion-S to obtain a first order estimation of the NE-Orion-S inclination. Assuming a proportional relation between the bar inclination with respect to the plane of the sky and the average distances with respect to the [O I] maximum emission of Table 2, we have estimated that the plane of the NE-Orion-S should be tilted about $48^\circ \pm 13^\circ$ with respect to the line of sight. This angle was calculated as a weighted average of the individual estimations for each emitting zone. In addition, it is impor-

tant to note that the NE-Orion-S has a complex structure of shadowed regions and other features as we see in Fig. 1 as well as in the new combined image of the Huygens region obtained by J.R. Walsh using a *drizzle* technique to produce a mosaic with a resolution of 0''.1 over the whole field³. Furthermore, the proximity and unknown exact position with respect to the Trapezium cluster is also playing a role on the geometry of what we observe as we mention in §5.1. Therefore, it can be difficult to interpret this ionization front as a simple slab with a given inclination. In this sense, our analysis of the individual spatial profiles extracted parallel to the main diagonal of the NE-Orion-S field can give further information about the complex structure of the NE-Orion-S. We have noted that the emission of [S II] and [O II] are much separated in the profiles extracted below—to the southeast of—the main diagonal than above it. In fact, we have estimated that the average distances between the emission peaks of [S II] and [O II] and that of [O I] are of about $0''.7 \pm 0''.4$ and $1''.9 \pm 0''.9$ below the main diagonal, and $0''.1 \pm 0''.3$ and $0''.6 \pm 0''.3$ above it. This fact suggests that the inclination of the NE-Orion-S is not constant along the observed field. Below the main diagonal, the plane of the NE-Orion-S seems to be less inclined with respect to the line of sight—more edge-on. But, above the main diagonal, the inclination angle is larger and the peaks of the line emission of the different ionic species can not be resolved. The variation of the inclination of the NE-Orion-S along the field may also explain the change of the width of the area of high [N II]/H α ratio—a good indicator of the inclination of an ionization front, as it is commented in §5.1— across the field (see Fig. 5), which seems to be wider below the main diagonal.

In Fig. 9 we have also plotted the spatial profiles of physical conditions of the BB and NE-Orion-S along the same diagonals as in the case of upper panels. Here, some of the results commented in §5.2 are more clearly seen: T_e ([N II]) is always higher than T_e ([O III]), but they tend to be more similar inside the bars. For the NE-Orion-S we can note a correlation between the n_e and T_e ([N II]) profiles, where lower temperatures are reached where the densities are higher. At the BB, this effect is not as clear as in the case of NE-Orion-S, this can be due to the lower densities of the BB.

6.2 Abundance discrepancy problem

The Orion Nebula is an unique object to analyse and explore particular problems in common with other H II regions. This is the case of the well known abundance discrepancy (AD) problem, *i.e.* the disagreement between the abundances of the same heavy-element ion derived from CELs and RLs. The AD problem is quantified making use of the AD factor, ADF, which can be defined for a given ion as

$$ADF(X^{i+}) = \log\left(\frac{X^{i+}}{H^+}\right)_{RL} - \log\left(\frac{X^{i+}}{H^+}\right)_{CEL}. \quad (2)$$

From intermediate and high resolution spectroscopy, several works have found that the $ADF(O^{2+})$ is always between 0.1 and 0.3 dex in Galactic and extragalactic H II

³ J.R. Walsh webpage: <http://www.stecf.org/~jwalsh/>

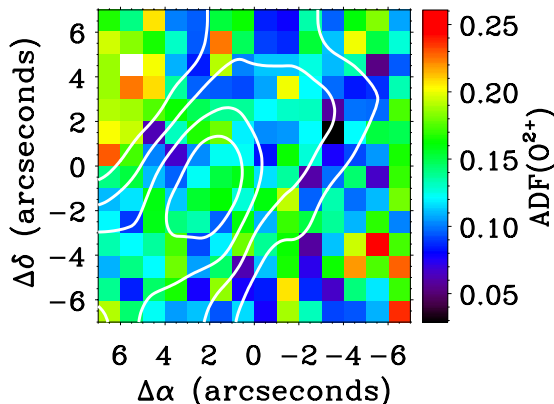


Figure 10. Spatial distribution of $\text{ADF}(\text{O}^{2+})$ for the NE-Orion-S with $\text{H}\alpha$ contours overplotted.

regions (see *e.g.* Esteban et al. 2002; Tsamis et al. 2003; Esteban et al. 2004; García-Rojas & Esteban 2007; López-Sánchez et al. 2007; Mesa-Delgado et al. 2008; Esteban et al. 2009; Mesa-Delgado & Esteban 2010). García-Rojas & Esteban (2007) argued that the AD problem in H II regions seems to be consistent with the predictions of the temperature fluctuation paradigm proposed by Peimbert (1967) and parametrized by the mean square of the spatial variations of temperature, the so-called t^2 parameter. Under this hypothesis, the AD would be produced by the very different temperature dependence of the emissivities of both kinds of lines and the abundances from RLs would be the representative ones of the ionized gas. However, the existence and origin of such temperature fluctuations are still controversial and the AD problem remains open. Other authors as Tsamis & Péquignot (2005) and Stasińska et al. (2007) have proposed a different hypothesis to explain the AD problem in H II regions. Based on the model for heavy-element mixing of Tenorio-Tagle (1996), Stasińska et al. (2007) propose that the presence of cold metal-rich droplets of supernova ejecta still not mixed with the ambient gas of the H II regions would produce most of the RL emission, while CEL emission would be produced by the ambient gas, which would have the expected composition of the local interstellar medium. In such case, the abundances from CELs would be the truly representative ones of the nebula. Recently, the studies performed in the Orion Nebula by Mesa-Delgado et al. (2009), Tsamis et al. (2011) and Simón-Díaz & Stasińska (2011) have provided new observational clues to address this puzzling issue. Mesa-Delgado et al. (2009) obtained echelle spectroscopy of the HH 202-S separating the kinematic component of the background emission from that of the gas flow finding clearly higher $\text{ADF}(\text{O}^{2+})$ values at the high-velocity component. This result suggests a possible relation between the $\text{ADF}(\text{O}^{2+})$ and the gas flow velocity. Tsamis et al. (2011) carried out a high-spectral resolution analysis of the protoplanetary disc LV2 with FLAMES. Their study of LV2 emission with the nebular background subtracted shows $\text{ADF}(\text{O}^{2+})$ values which are basically zero. This surprising result seems to be related to the high electron densities expected in these kind of objects, which affect the ionic abundances derived from CELs. Therefore, it is necessary to explore the behaviour of the $\text{ADF}(\text{O}^{2+})$ in other morpholog-

ical structures of the Orion Nebula –as stratified ionization fronts– in order to better understand and constrain the AD problem. Finally, we consider important to comment the recent remarkable result by Simón-Díaz & Stasińska (2011), who find that the nebular oxygen total abundances derived from RLs agrees better with the stellar abundances of B-type stars of the Orion Association than those determined from CELs. This result is an indication that nebular abundances obtained from RLs may be more reliable than those derived from the standard method based on CELs and therefore stressing the importance of investigating the AD problem.

As we pointed out in §5.3 we derived O^{2+} abundances from RLs in the NE-Orion-S field. Subtracting these abundances from those obtained from CELs (Fig. 7) we find the spatial distribution of the $\text{ADF}(\text{O}^{2+})$, which is presented in Fig. 10. As we can see, the $\text{ADF}(\text{O}^{2+})$ seems to be slightly higher at the northeast corner of the field, but the map does not show any remarkable structure inside the ionization front. The range of the variations goes from 0.05 to 0.25 dex with a typical error of about 0.12 dex for each spaxel. However, we have checked that the extreme values of the $\text{ADF}(\text{O}^{2+})$ correspond typically with spaxels with low signal-to-noise ratio in the O II RLs of their spectra. Therefore, not particular variations of the $\text{ADF}(\text{O}^{2+})$ are related to the presence of stratified ionization fronts, at least with the properties and physical conditions of the NE-Orion-S and the spatial resolution of our observations. The mean value of the $\text{ADF}(\text{O}^{2+})$ in the field is about 0.14 dex with a standard deviation of about 0.05 dex. Therefore, there is a real difference between the O^{2+} abundances from RLs and CELs, which is in the range between 21% and 44%. This is precisely the value found in our previous studies of the Orion Nebula (*e.g.* Esteban et al. 2004; Mesa-Delgado et al. 2008).

7 CONCLUSIONS

In this paper we analyse integral field optical spectroscopy of two two remarkable structures related to ionization fronts of the Orion Nebula: the Bright Bar (BB) and the northeast edge of the Orion South cloud (NE-Orion-S). In both fields, we have mapped emission line fluxes and ratios, physical conditions and chemical abundances at spatial scales of $1''$.

The maps clearly show the ionization stratification of both ionization fronts, which present rather different inclination angles as well as different distances with respect to $\theta^1 \text{ Ori C}$, the main exciting source of the nebula. The ionization structure of the BB is well resolved because the ionization front is almost edge-on –inclination angle of 7° with respect to the line of sight–, while the NE-Orion-S is a portion of the Orion-S cloud suspended within the main body of the nebula, which is more tilted and presents a more complex structure. We have analysed spatial profiles of selected emission lines of ions with different ionization potential and estimated the average distances of the peaks of the emission of these lines with respect to the maximum of [O I]. Comparing those distances in both fronts, we have estimated that the plane of the NE-Orion-S field could be tilted about $48^\circ \pm 13^\circ$ with respect to the line of sight. However, the distances between the peaks of the lines with respect to [O I] change in the different spatial profiles extracted for the NE-Orion-S,

indicating that the inclination angle of this ionization front should vary across the observed field.

The maps of electron density, $n_e(\text{S II})$, show that NE-Orion-S is much denser than the BB. The NE-Orion-S has a mean density of about 10900 cm^{-3} , while the BB has 4370 cm^{-3} . In both cases, the $[\text{S II}]$ lines may be somewhat affected by collisional de-excitation because the nominal values of n_e we find are of the order of their critical densities. In any case, this de-excitation should not be severe due to the rather similar n_e we determine from $[\text{Fe III}]$ lines. The structure of the temperature maps are rather featureless and $T_e(\text{N II})$ is usually higher than $T_e(\text{O III})$, specially outside the bars. The maps of total O abundance show mean values consistent with previous determinations of the literature for the Orion Nebula, but they show a pattern very similar to the maps of O^+/H^+ ratio and $n_e(\text{S II})$. The spaxels with higher n_e values also show higher O^+ and O abundances. We find that considering values of n_e slightly lower than those determined from the $[\text{S II}]$ line ratio –but of the order of the quoted uncertainties– the problem can be satisfactorily solved.

Finally, the higher signal-to-noise ratio of the spectra in the NE-Orion-S field allows us to detect, measure and map the faint RLs of O II and C II. We explore the abundance discrepancy problem in this field comparing the O^{2+} abundance maps derived from CELs and RLs, finding a featureless spatial distribution for the abundance discrepancy factor of O^{2+} , $\text{ADF}(\text{O}^{2+})$, which shows values ranging between 0.05 and 0.25 dex with a typical error of about 0.12 dex. The mean $\text{ADF}(\text{O}^{2+})$ is 0.14 ± 0.05 dex, in excellent agreement with other previous determinations in other areas of the Orion Nebula –except at Herbig-Haro objects (Mesa-Delgado et al. 2008, 2009) and the LV2 protoplanetary disc (Tsamis et al. 2011). This result implies that the O^{2+} abundances from RLs are between 21% and 44% larger than those from CELs and that there is not any particular variation of the $\text{ADF}(\text{O}^{2+})$ related to the presence of stratified ionization fronts, at least for the properties and physical conditions of the NE-Orion-S and the spatial resolution of our observations

ACKNOWLEDGMENTS

We are very grateful to the referee of this paper, C.R. O'Dell, for his useful comments and suggestions. We also thank W. Henney, C. Morriset and Y. Tsamis their helpful comments and correspondence. This work has been funded by the Ministerio de Educación y Ciencia (MEC) under project AYA2007-63030.

REFERENCES

- Baldwin J. A., Ferland G. J., Martin P. G., Corbin M. R., Cota S. A., Peterson B. M., Slettebak A., 1991, *ApJ*, 374, 580
- Balick B., Gammon R. H., Hjellming R. M., 1974, *PASP*, 86, 616
- Bally J., O'Dell C. R., McCaughrean M. J., 2000, *AJ*, 119, 2919
- Blagrove K. P. M., Martin P. G., Baldwin J. A., 2006, *ApJ*, 644, 1006
- Blagrove K. P. M., Martin P. G., Rubin R. H., Dufour R. J., Baldwin J. A., Hester J. J., Walter D. K., 2007, *ApJ*, 655, 299
- Costero R., Peimbert M., 1970, *Boletín de los Observatorios Tonantzintla y Tacubaya*, 5, 229
- Davey A. R., Storey P. J., Kisieliński R., 2000, *A&AS*, 142, 85
- Doi T., O'Dell C. R., Hartigan P., 2004, *AJ*, 127, 3456
- Esteban C., Bresolin F., Peimbert M., García-Rojas J., Peimbert A., Mesa-Delgado A., 2009, *ApJ*, 700, 654
- Esteban C., Peimbert M., García-Rojas J., Ruiz M. T., Peimbert A., Rodríguez M., 2004, *MNRAS*, 355, 229
- Esteban C., Peimbert M., Torres-Peimbert S., Escalante V., 1998, *MNRAS*, 295, 401
- Esteban C., Peimbert M., Torres-Peimbert S., Rodríguez M., 2002, *ApJ*, 581, 241
- García-Díaz M. T., Henney W. J., 2007, *AJ*, 133, 952
- García-Díaz M. T., Henney W. J., López J. A., Doi T., 2008, *Rev. Mexicana Astron. Astrofis.*, 44, 181
- García-Rojas J., Esteban C., 2007, *ApJ*, 670, 457
- García-Rojas J., Peña M., Peimbert A., 2009, *A&A*, 496, 139
- Hester J. J., 1991, *PASP*, 103, 853
- Hester J. J., Gilmozzi R., O'dell C. R., Faber S. M., Campbell B., Code A., Currie D. G., Danielson G. E., Ewald S. P., Groth E. J., Holtzman J. A., Kelsall T., Lauer T. R., Light R. M., Lynds R., O'Neil Jr. E. J., Shaya E. J., Westphal J. A., 1991, *ApJ*, 369, L75
- Hohenkerk C. Y., Sinclair A. T., 1985, *The Computation of Angular Atmospheric Refraction at Large Zenith Angles*. Royal Greenwich Observatory
- Johansson S., Zethson T., Hartman H., Ekberg J. O., Ishibashi K., Davidson K., Gull T., 2000, *A&A*, 361, 977
- Kassis M., Adams J. D., Campbell M. F., Deutsch L. K., Hora J. L., Jackson J. M., Tollestrup E. V., 2006, *ApJ*, 637, 823
- López-Sánchez A. R., Esteban C., García-Rojas J., Peimbert M., Rodríguez M., 2007, *ApJ*, 656, 168
- Marconi A., Testi L., Natta A., Walmsley C. M., 1998, *A&A*, 330, 696
- Mesa-Delgado A., Esteban C., 2010, *MNRAS*, 405, 2651
- Mesa-Delgado A., Esteban C., García-Rojas J., 2008, *ApJ*, 675, 389
- Mesa-Delgado A., Esteban C., García-Rojas J., Luridiana V., Bautista M., Rodríguez M., López-Martín L., Peimbert M., 2009, *MNRAS*, 395, 855
- Mesa-Delgado A., López-Martín L., Esteban C., García-Rojas J., Luridiana V., 2009, *MNRAS*, 394, 693
- O'Dell C. R., 2001, *PASP*, 113, 29
- O'Dell C. R., Henney W. J., 2008, *AJ*, 136, 1566
- O'Dell C. R., Henney W. J., Abel N. P., Ferland G. J., Arthur S. J., 2009, *AJ*, 137, 367
- O'Dell C. R., Peimbert M., Peimbert A., 2003, *AJ*, 125, 2590
- O'Dell C. R., Wong K., 1996, *AJ*, 111, 846
- O'Dell C. R., Yusef-Zadeh F., 2000, *AJ*, 120, 382
- Oke J. B., 1990, *AJ*, 99, 1621
- Osterbrock D. E., Ferland G. J., 2006, *Astrophysics of gaseous nebulae and active galactic nuclei*. 2nd. ed. Sausalito, CA: University Science Books

- Peimbert A., Peimbert M., 2005, in Torres-Peimbert D., MacAlpine G., eds, *Rev. Mexicana Astron. Astrofis. Conf. Ser. Vol. 23, Oxygen Recombination Line Abundances in Gaseous Nebulae*. p. 9
- Peimbert M., 1967, *ApJ*, 150, 825
- Pellegrini E. W., Baldwin J. A., Ferland G. J., Shaw G., Heathcote S., 2009, *ApJ*, 693, 285
- Pogge R. W., Owen J. M., Atwood B., 1992, *ApJ*, 399, 147
- Quinet P., 1996, *A&AS*, 116, 573
- Roth M. M., Kelz A., Fechner T., Hahn T., Bauer S.-M., Becker T., Böhm P., Christensen L., Dionies F., Paschke J., Popow E., Wolter D., Schmoll J., Laux U., Altmann W., 2005, *PASP*, 117, 620
- Rubin R. H., Martin P. G., Dufour R. J., Ferland G. J., Blagrove K. P. M., Liu X.-W., Nguyen J. F., Baldwin J. A., 2003, *MNRAS*, 340, 362
- Rubin R. H., Simpson J. P., Haas M. R., Erickson E. F., 1991, *ApJ*, 374, 564
- Sánchez S. F., Cardiel N., Verheijen M. A. W., Martín-Gordón D., Vilchez J. M., Alves J., 2007, *A&A*, 465, 207
- Seidelmann P. K., 1992, *Explanatory Supplement to the Astronomical Almanac*. University Science Books
- Shaw R. A., Dufour R. J., 1995, *PASP*, 107, 896
- Simón-Díaz S., Herrero A., Esteban C., Najarro F., 2006, *A&A*, 448, 351
- Simón-Díaz S., Stasińska G., 2011, *A&A*, 526, A48
- Stasińska G., Tenorio-Tagle G., Rodríguez M., Henney W. J., 2007, *A&A*, 471, 193
- Storey P. J., 1994, *A&A*, 282, 999
- Storey P. J., Hummer D. G., 1995, *MNRAS*, 272, 41
- Tauber J. A., Tielens A. G. G. M., Meixner M., Foldsmith P. F., 1994, *ApJ*, 422, 136
- Tenorio-Tagle G., 1996, *AJ*, 111, 1641
- Tielens A. G. G. M., Meixner M. M., van der Werf P. P., Bregman J., Tauber J. A., Stutzki J., Rank D., 1993, *Science*, 262, 86
- Tsamis Y. G., Barlow M. J., Liu X.-W., Danziger I. J., Storey P. J., 2003, *MNRAS*, 338, 687
- Tsamis Y. G., Péquignot D., 2005, *MNRAS*, 364, 687
- Tsamis Y. G., Walsh J. R., Vilchez J. M., Péquignot D., 2011, *MNRAS*, 412, 1367
- van der Werf P. P., Stutzki J., Sternberg A., Krabbe A., 1996, *A&A*, 313, 633
- van der Wiel M. H. D., van der Tak F. F. S., Ossenkopf V., Spaans M., Roberts H., Fuller G. A., Plume R., 2009, *A&A*, 498, 161
- Vasconcelos M. J., Cerqueira A. H., Plana H., Raga A. C., Morisset C., 2005, *AJ*, 130, 1707
- Walmsley C. M., Natta A., Oliva E., Testi L., 2000, *A&A*, 364, 301
- Walsh J. R., Roy J. R., 1990, in D. Baade & P. J. Grosbol ed., *European Southern Observatory Conference and Workshop Proceedings Vol. 34, Area Spectroscopy and Correction for Differential Atmospheric Refraction*. p. 95
- Walter D. K., Dufour R. J., Hester J. J., 1992, *ApJ*, 397, 196
- Walter D. K., Dufour R. J., Hester J. J., 1993, *Rev. Mexicana Astron. Astrofis.*, 27, 207
- Wen Z., O'Dell C. R., 1995, *ApJ*, 438, 784
- Young Owl R. C., Meixner M. M., Wolfire M., Tielens A. G. G. M., Tauber J., 2000, *ApJ*, 540, 886
- Zhang H., 1996, *A&AS*, 119, 523
- Zuckerman B., 1973, *ApJ*, 183, 863